Prepared for submission to JHEP

BARI-TH/2013-673
FTUAM-13-4

Low-energy photon and pion scattering in holographic QCD

Pietro Colangelo,[1] **Juan Jose Sanz-Cillero,**[2] **Fen Zuo**[1]

[1] *Istituto Nazionale di Fisica Nucleare, Sezione di Bari, Italy*

[2] *Departamento de Física Teórica, Universidad Autónoma de Madrid, Cantoblanco, 28049 Madrid, Spain*

E-mail: Pietro.Colangelo@ba.infn.it, juanj.sanz@uam.es, Fen.Zuo@ba.infn.it

Abstract: Using holographic models where chiral symmetry is broken through IR b.c.'s, we determine a novel set of relations between QCD matrix elements. In particular, we find that the amplitudes of the three processes $\pi\pi \to \pi\pi$, $\gamma\gamma \to \pi\pi$ and $\gamma \to \pi\pi\pi$ involve a single scalar function $h(Q^2)$ given by a suitable 5D integral of the EoM Green's function. In a phenomenological analysis of $\gamma\gamma \to \pi\pi$ we find an overall agreement with the experimental cross section for a broad range of energy. Moreover, the polarizabilities at low energies show a fair agreement between the holographic approach, previous computations and experiment.

Keywords: AdS-CFT Correspondence, Chiral Lagrangians, $1/N$ Expansion, QCD

Contents

1 Introduction

Inspired by a holographic analysis of the axial-vector-vector (AVV) and left-right (LR) quark current Green's functions [1], several investigations have been devoted to the possible interplay between the anomalous and even intrinsic-parity sectors of Quantum Chromodynamics [2–8]. In a recent study [9], using holographic models where chiral symmetry is realized nonlinearly through boundary conditions (b.c.'s) [10–13], we derived a series of novel form factor and low-energy constant (LEC) relations in the limit of large number of colors $N_C \to \infty$ [14]. Here we continue along that line, and extend the analysis to scattering processes, going beyond the realm of static properties (mass spectra and couplings) and facing the more difficult dynamical problem of two-body scattering amplitudes. We focus on $\pi\pi$–scattering and on the radiative processes $\gamma\gamma \to \pi\pi$ and $\gamma \to 3\pi$, finding that it is possible to describe the three amplitudes through a single function determined by an appropriate 5D integral of the Green's function of the five-dimensional equations of motion (EoM).

Chiral Perturbation theory (χPT) is the effective field theory describing the low-energy interaction of the pseudo-Goldstone bosons which emerge from the spontaneous breaking

of the chiral symmetry [15, 16]. The observables are obtained by a perturbative expansion in terms of the external momenta and the pseudoscalar mass, and involve a set of effective couplings [17–20]. However, these couplings of the low-energy theory are not fixed by the symmetry, but need to be determined through other procedures. In [9] we considered a set of holographic models without explicit chiral symmetry breaking, and computed all the LEC's of the $\mathcal{O}(p^6)$ χPT Lagrangian in the absence of scalar-pseudoscalar sources. As the LEC's are independent of the quark masses, our results for the chiral couplings remain valid in the massive quark case.

Here, using the $\mathcal{O}(p^6)$ LEC determinations in [9], we carry out a phenomenological analysis of the $\gamma\gamma \to \pi\pi$ reaction, as this matrix element depends on a transparent way on the $\mathcal{O}(p^6)$ LEC's [21–23]. We also study the low-energy polarizabilities $(\alpha_1 + \beta_1)$ and $(\alpha_2 \pm \beta_2)$, defined below, whose lowest chiral orders are determined by the pion Born term and the $\mathcal{O}(p^4)$ one-loop alone, with no contribution from $\mathcal{O}(p^4)$ LEC's [24]. The first tree-level contribution (in addition to the pion Born term) occurs at $\mathcal{O}(p^6)$. Indeed, the polarizabilities $(\alpha_1 + \beta_1)$ and $(\alpha_2 + \beta_2)$ vanish at $\mathcal{O}(p^2)$ and $\mathcal{O}(p^4)$, starting the first non-vanishing contribution at $\mathcal{O}(p^6)$. All this makes these observables an interesting benchmark for the $\mathcal{O}(p^6)$ LEC determination in [9]. We find that the relevant combinations of chiral couplings are fully determined by the anomalous Chern-Simons action and are universal for this kind of holographic models, since they are independent of the details of the 5D background [9]. In addition, we observe that the experimental $\gamma\gamma \to \pi\pi$ cross section is reproduced even in the region away from the threshold.

The article is organized as follows. In Sec. 2 we recall the holographic setup used to calculate the LEC and their relations. In Sec. 3 we show that a unique function appears in several $\pi\pi$ and $\gamma\gamma$ scattering amplitudes, so that relations can be worked out among these amplitudes and they can be experimentally tested. In Sec. 4 we study the polarizabilities in $\gamma\gamma \to \pi\pi$ scattering, and compare the results obtained in our holographic approach to a few experimental and theoretical determinations. Then, we draw our conclusions.

2 Holographic setup

We restrict ourselves to a class of holographic models where chiral symmetry is realized nonlinearly, through suitable boundary conditions. This class of models was proposed in ref. [10], developed in refs. [11–13], and further studied in refs. [1, 9]. The gauge group is $U(n_f)$, and the $5D$ action is composed by the Yang–Mills (YM) and Chern–Simons (CS) terms, describing the intrinsic even-parity and the anomalous QCD sectors, respectively [10–13]:

$$S = S_{\rm YM} + S_{\rm CS} \tag{2.1}$$

with

$$S_{\rm YM} = -\int d^5x \ {\rm Tr}\left[-f^2(z)\mathcal{F}_{z\mu}^2 + \frac{1}{2g^2(z)}\mathcal{F}_{\mu\nu}^2\right], \tag{2.2}$$

$$S_{\rm CS} = -\kappa \int {\rm Tr}\left[\mathcal{A}\mathcal{F}^2 + \frac{i}{2}\mathcal{A}^3\mathcal{F} - \frac{1}{10}\mathcal{A}^5\right]. \tag{2.3}$$

The fifth coordinate z runs from $-z_0$ to z_0, with $0 < z_0 \leq +\infty$. $\mathcal{A}(x,z) = \mathcal{A}_M dx^M$ is the 5D gauge field and $\mathcal{F} = d\mathcal{A} - i\mathcal{A} \wedge \mathcal{A}$ the field strength. In terms of the $U(n_f)$ generators t^a, normalized as $Tr[t^a t^b] = \delta^{ab}/2$, they read: $\mathcal{A} = \mathcal{A}^a t^a$ and $\mathcal{F} = \mathcal{F}^a t^a$. The coefficient $\kappa = N_C/(24\pi^2)$ is fixed by the chiral anomaly of QCD [25, 26].

If the functions $f^2(z)$ and $g^2(z)$ in (2.2) are invariant under reflection $z \to -z$, parity can be properly defined in these models. In appendix B we provide the profiles of $f(z)$ and $g(z)$ for the flat metric [10], "Cosh" [10], Hard-Wall [12] and Sakai-Sugimoto models [11, 13] that are used below.

As discussed in details in ref. [9], in (2.1) the QCD chiral symmetry is promoted to a 5D gauge symmetry, with the possibility of naturally introducing the right- and left-handed current sources, $r_\mu(x)$ and $\ell_\mu(x)$ respectively. The Goldstone bosons are contained in the $\mathcal{A}_z$ component of the gauge field, and are described through the chiral field U, given by the Wilson line

$$U(x^\mu) = \mathrm{P}\exp\left\{ i \int_{-z_0}^{+z_0} \mathcal{A}_z(x^\mu, z') dz' \right\}. \tag{2.4}$$

This field transforms as

$$U(x) \to g_R(x) U(x) g_L^\dagger(x) \tag{2.5}$$

with $g_L(x)$ and $g_R(x)$ the left and right gauge transformations localized at $z = -z_0$ and $z = z_0$, respectively. The $\mathcal{A}_\mu$ components of the gauge fields contain vector and axial-vector resonances, since

$$\mathcal{A}_\mu(x,z) = \ell_\mu(x)\psi_-(z) + r_\mu(x)\psi_+(z) + \sum_{n=1}^{\infty} B_\mu^{(n)}(x)\psi_n(z)\,. \tag{2.6}$$

The ultraviolet (UV) boundary conditions

$$\mathcal{A}_\mu(x,-z_0) = \ell_\mu(x)\,, \qquad\qquad \mathcal{A}_\mu(x,z_0) = r_\mu(x) \tag{2.7}$$

are imposed. In Eq.(2.6) the functions $\psi_\pm(z) = \frac{1}{2}(1 \pm \psi_0(z))$ are determined by the $\psi_0(z)$ solution of the 5D EoM of the $\mathcal{A}_\mu(x,z)$ gauge fields corresponding to the zero mode, with b.c.'s $\psi_0(\pm z_0) = \pm 1$. On the other hand, the $\psi_n(z)$ correspond to the resonant modes with mass m_n; their b.c.'s are $\psi_n(\pm z_0) = 0$. Under a suitable gauge transformation it is possible to set $\mathcal{A}_z = 0$, with the space-time components of the 5D field taking the form

$$\mathcal{A}_\mu(x,z) = i\Gamma_\mu(x) + \frac{u_\mu(x)}{2}\psi_0(z) + \sum_{n=1}^{\infty} v_\mu^n(x)\psi_{2n-1}(z) + \sum_{n=1}^{\infty} a_\mu^n(x)\psi_{2n}(z)\,, \tag{2.8}$$

where the tensors $u_\mu(x)$ and $\Gamma_\mu(x)$, commonly used in χPT [17, 18, 27, 28], naturally show up:

$$u_\mu(x) \equiv \mathrm{i}\left\{ \xi_R^\dagger(x)\left(\partial_\mu - \mathrm{i}r_\mu\right)\xi_R(x) - \xi_L^\dagger(x)\left(\partial_\mu - \mathrm{i}\ell_\mu\right)\xi_L(x) \right\} \tag{2.9}$$

$$\Gamma_\mu(x) \equiv \frac{1}{2}\left\{ \xi_R^\dagger(x)\left(\partial_\mu - \mathrm{i}r_\mu\right)\xi_R(x) + \xi_L^\dagger(x)\left(\partial_\mu - \mathrm{i}\ell_\mu\right)\xi_L(x) \right\}, \tag{2.10}$$

with the non-linear realization $u(x) = \xi_R(x) = \xi_L^\dagger(x) = \exp\{i\pi^a t^a/F\}$.

The 5D action can be expressed using the decomposition (2.8) of the 5D gauge fields in resonances and the non-linearly realized chiral Goldstone bosons [9, 11–13]. The resulting 4D action terms relevant for our analysis contain operators with only Goldstones (see appendix A) and pieces with one resonance field v_μ^n, together with the couplings $b_{v^n\pi\pi}$, c_{v^n} and d_{v^n}:

$$S_{\rm YM}\Big|_{1-res} = -\sum_n \frac{i\, b_{v^n\pi\pi}}{4} \int {\rm d}^4x \langle\, (\nabla_\mu v_\nu^n - \nabla_\nu v_\mu^n)[u^\mu, u^\nu]\,\rangle \;\; + \;\; ... \tag{2.11}$$

$$S_{\rm CS}\Big|_{1-res} = \sum_n \epsilon^{\mu\nu\alpha\beta} \int {\rm d}^4x \left[-\frac{N_C}{32\pi^2} c_{v^n} \langle\, u_\mu \{v_\nu^n, f_{+\alpha\beta}\}\,\rangle + \frac{iN_C}{16\pi^2}\,(c_{v^n} - d_{v^n}) \langle\, v_\mu^n u_\nu u_\alpha u_\beta\,\rangle \right] + \; ... \tag{2.12}$$

with $v_\mu^n = v_\mu^{n,a}\, t^a$ and the covariant tensor $f_+^{\alpha\beta} = \xi_R^\dagger F_R^{\alpha\beta} \xi_R + \xi_L^\dagger F_L^{\alpha\beta} \xi_L$ provided by the left and right source field-strength tensors [17, 18, 27, 28]. The couplings are given by the integrals of the corresponding 5D wave functions:

$$\begin{aligned} b_{v^n\pi\pi} &= \int_{-z_0}^{z_0} \frac{\psi_{2n-1}(z)\,(1-\psi_0(z)^2)}{g^2(z)}\,{\rm d}z\,, \\ c_{v^n} &= -\frac{1}{2}\int_{-z_0}^{z_0} \psi_0(z)\,\psi'_{2n-1}(z){\rm d}z\,, \\ d_{v^n} &= \frac{1}{2}\int_{-z_0}^{z_0} \psi_0(z)^2\,\psi'_0(z)\,\psi_{2n-1}(z)\,{\rm d}z\,. \end{aligned} \tag{2.13}$$

The primes denote derivative with respect to z. Using the EoM of $\psi_n(z)$ the relation

$$c_{v^n} = g_{v^n\pi\pi} \tag{2.14}$$

is obtained [9, 13], with $g_{v^n\pi\pi} = \dfrac{m_{v^n}^2}{2F^2} b_{v^n\pi\pi}$ the coupling between the vector resonance v^n and a pion pair. This equation implies a connection between the $v^n \to \pi\pi$ and $v^n \to \pi\gamma$ decay widths which are determined by the couplings $g_{v^n\pi\pi}$ and c_{v^n}, respectively, and represents the key ingredient for the relations between amplitudes exploited in the following. Another important property in the considered models is that the vertex $a^n\pi\gamma$ vanishes [9, 12], therefore all the amplitudes studied below do not get contributions from the axial-vector resonances.

One may wonder whether the relation (2.14) is experimentally fulfilled. The experimental results for the lightest vector mesons are [13]

$$c_\omega|_{\rm exp} \;=\; 5.80\;, \qquad\qquad g_{\rho\pi\pi}|_{\rm exp} \;=\; 5.99\;, \tag{2.15}$$

determined from the measured $\omega \to \pi^0\gamma$ and $\rho \to \pi\pi$ decay rates, respectively [29]. On the other hand, in the holographic analysis in ref. [9] we found for the considered 5D models the results in Table 1, all close to the experimental data. In each case and all along the paper, the mass of the lightest vector meson $m_\rho = 776$ MeV and the pion decay constant $F = 87$ MeV are taken as inputs to set the parameters of the 5D model [9]. Since the action (2.1) does not incorporate quark masses, all the interaction vertices are predicted in

the chiral limit. This allows us to extract some relevant combinations of LEC's, as they are quark mass independent. However, in the computation of cross sections and decay widths we consider the physical pion mass in the phase-space factors, assuming that this captures the most important quark mass corrections. Likewise, no scalar states or resonances with spin $S \geq 2$ are included in the present analysis.

	Flat	Cosh	Hard-Wall	Sakai-Sugimoto
$g_{\rho\pi\pi} = c_\rho$	5.11	5.14	5.13	5.11

Table 1. Couplings $g_{\rho\pi\pi}$ and c_ρ determined in four holographic QCD models.

3 Holographic description of scattering amplitudes

3.1 $\pi\pi$ scattering

The $\pi^a\pi^b \to \pi^c\pi^d$ scattering amplitude is provided by the isospin decomposition

$$A(\pi^a\pi^b \to \pi^c\pi^d) = A(s,t,u)\delta^{ab}\delta^{cd} + A(t,s,u)\delta^{ac}\delta^{bd} + A(u,t,s)\delta^{ad}\delta^{bc}\,, \tag{3.1}$$

with $s = (p_a+p_b)^2$, $t = (p_a-p_c)^2$, $u = (p_a-p_d)^2$ and the Mandelstam relation $s+t+u = 0$ in the massless pion limit. The holographic action yields the $v^n\pi\pi$ Lagrangian (2.11), in addition to direct $\pi\pi \to \pi\pi$ vertices, giving the amplitude

$$\begin{aligned} A(s,t,u) &= \frac{s}{F^2} + \frac{4L_1((t-u)^2-3s^2)}{F^4} + \sum_n \frac{b^2_{v^n\pi\pi}}{4F^4}\left[\frac{t^2(t+2s)}{m^2_{v^n}-t} + \frac{u^2(u+2s)}{m^2_{v^n}-u}\right] \\ &= \sum_n g^2_{v^n\pi\pi}\left[\frac{t+2s}{m^2_{v^n}-t} + \frac{u+2s}{m^2_{v^n}-u}\right] \end{aligned} \tag{3.2}$$

obtained using the definition of $g_{v^n\pi\pi}$ together with the sum rules [9, 12]

$$\sum_n b^2_{v^n\pi\pi} = 32L_1 \quad , \quad \sum_n b^2_{v^n\pi\pi} m^2_{v^n} = \frac{4F^2}{3}\,. \tag{3.3}$$

It is possible to express the $\pi\pi$–scattering amplitude (3.2) in a holographic form,

$$\begin{aligned} A(s,t,u) &= \frac{1}{4}\int_{-z_0}^{z_0} dz \int_{-z_0}^{z_0} dz'\ \psi_0'(z)\psi_0'(z')\left[(t+2s)\,G(-t;z,z') + (u+2s)\,G(-u;z,z')\right] \\ &= \frac{1}{4}\left[(t+2s)\,h(-t) + (u+2s)\,h(-u)\right], \end{aligned} \tag{3.4}$$

in terms of the function $h(Q^2)$ obtained from the integral of the Green's function $G(Q^2;z,z')$ in the z (holographic) coordinate:

$$h(Q^2) = \int_{-z_0}^{z_0} dz \int_{-z_0}^{z_0} dz'\,\psi_0'(z)\psi_0'(z')\,G(Q^2;z,z')\,, \tag{3.5}$$

$$G(Q^2;z,z') = \sum_{n=1}^{\infty} \frac{\psi_n(z)\psi_n(z')}{m_n^2+Q^2}\,. \tag{3.6}$$

To rewrite (3.2) into (3.4) we made use of the relation in Eq. (2.14). It is useful to express the $h(Q^2)$ function in terms of resonance exchanges,

$$h(Q^2) = \sum_n \frac{4g_{v^n\pi\pi}^2}{m_{v^n}^2 + Q^2} \;\; = \;\; \sum_n \frac{4c_{v^n}^2}{m_{v^n}^2 + Q^2} \, . \tag{3.7}$$

With the help of the sum-rules (3.3) the low-energy expansion can be worked out:

$$h(Q^2) = \frac{4}{3F^2} - \frac{32L_1Q^2}{F^4} + \frac{32(C_1+4C_3)Q^4}{F^4} + \mathcal{O}(Q^6) \, . \tag{3.8}$$

We also used the $\mathcal{O}(p^6)$ relations $(C_1 + 4C_3) = (3C_3 + C_4) = \sum_n F^4 g_{v^n\pi\pi}^2/(8m_{v^n}^6)$ derived in [9]. The right low-energy expansion of the $\pi\pi$–scattering amplitude at large N_C [16, 30] is recovered,

$$A(s,t,u)^{\chi\rm PT} = \frac{s}{F^2} + \frac{8L_1\,(t^2+u^2-2s^2)}{F^4} - \frac{8(C_1+4C_3)(t+u)(t^2+tu+u^2)}{F^4} + \mathcal{O}(p^8) \, . \tag{3.9}$$

Notice that, in the large-N_C limit, in the absence of other resonances, L_2 and L_3 are both related to the low-energy constant L_1 [27]: $L_2/2 = -L_3/6 = L_1$. In a similar way, at large–N_C one has $C_2 = 0$ and $(C_1 + 4C_3) = (3C_3 + C_4)$ when just vector resonance exchanges are taken into account [28, 31]. This result provides a consistency check of the holographic derivation and of the determination in [9] of the $\mathcal{O}(p^6)$ low energy constants.

The large-Q^2 behavior of the function $h(Q^2)$ also determines the high energy behavior of the scattering amplitudes. This can be obtained from the resonance expression (3.7), and depends on the convergence of the sum

$$\mathcal{H} \equiv \sum_{n=0}^{\infty} c_{v^n}^2 \;\; . \tag{3.10}$$

As long as this sum converges, one has

$$h(Q^2) \quad \stackrel{Q^2\to\infty}{\longrightarrow} \quad \frac{4\mathcal{H}}{Q^2} \;\; . \tag{3.11}$$

Using the holographic expression for c_{v^n}, we can rewrite the sum as a 5D integral,

$$\mathcal{H} = \frac{1}{4}\int_{-z_0}^{z_0} [\psi_0'(z)]^2 \; g^2(z) \mathrm{d}z = \frac{F^4}{16}\int_{-z_0}^{z_0} \frac{g^2(z)}{f^4(z)} \mathrm{d}z \;\; . \tag{3.12}$$

For arbitrary background functions $f^2(z)$ and $g^2(z)$ this integral may diverge. However, if we restrict ourselves to the case when the kinetic coefficient H_1 of the external sources in the $\mathcal{O}(p^4)$ χPT Lagrangian is UV–divergent [1], we can prove in general that $\mathcal{H}$ is finite, as shown in appendix A. This is true for all the models listed in appendix B, although the explicit values of the resonance parameters and of the sum are different in each case. For example, one has $\mathcal{H} = g_5^2/2 = 4m_\rho^2/(\pi^2F^2)$ and $\mathcal{H} = g_5^2/3 = m_\rho^2/(3F^2)$ for the Flat

[1] This requirement is not fulfilled in the flat model, but $\mathcal{H}$ is still finite in this model.

and "Cosh" models, respectively. It is interesting to remark that, contrary to other matrix elements such as the two-point vector current correlation function, the short-distance power behavior is similar for models with very different backgrounds near the UV boundary. The reason may be that only when we take the momentum square of the external source to be large, as we usually do in the vector correlator and in form factors involving pions, we probe the ultraviolet region of the backgrounds. For instance, in the isospin $I = 2$ channel one has $T^2(s,t,u) = A(t,s,u) + A(u,t,s)$, and the large-$s$ behaviour of the corresponding $J = 0$ partial wave is

$$T_0^2(s) = -\frac{1}{64\pi s}\int_{-s}^{0}(t+2s)\,h(-t)\,dt \quad \stackrel{s\to\infty}{\longrightarrow} \quad -\frac{\mathcal{H}}{8\pi}\ln\frac{s}{\Lambda^2} + \mathcal{O}(s^0)\,. \tag{3.13}$$

The parameter Λ is a finite hadronic scale arising from the integration. Thus, the residual logarithmic behavior found at high energies in the case of a finite number of vector exchanges [31, 32] shows up also in holographic models, with an infinite tower of resonances. Calculations of higher partial waves give a similar logarithmic behavior.

3.2 $\gamma\gamma \to \pi\pi$ scattering

We now analyze an observable for which the odd intrinsic-parity sector of the action plays a crucial role, the radiative process $\gamma\gamma \to \pi\pi$. We first perform a separate theoretical study of the neutral and charged modes. Nonetheless, our holographic description provides pretty similar structures for both of them.

3.2.1 $\gamma\gamma \to \pi^0\pi^0$

The $\gamma(k_1,\epsilon_1)\gamma(k_2,\epsilon_2) \to \pi^0(p_1)\pi^0(p_2)$ scattering amplitude is described by two structure functions, $A(s,t,u)^{\gamma\gamma\to\pi^0\pi^0}$ and $B(s,t,u)^{\gamma\gamma\to\pi^0\pi^0}$:

$$T^{\gamma\gamma\to\pi^0\pi^0} = e^2(\epsilon_1^\mu\epsilon_2^\nu T^{(1)}_{\mu\nu}) \times A(s,t,u)^{\gamma\gamma\to\pi^0\pi^0} \;+\; e^2(\epsilon_1^\mu\epsilon_2^\nu T^{(2)}_{\mu\nu}) \times B(s,t,u)^{\gamma\gamma\to\pi^0\pi^0}\,. \tag{3.14}$$

The Lorentz structures are defined as $(\epsilon_1^\mu\epsilon_2^\nu T^{(1)}_{\mu\nu}) = \frac{s}{2}(\epsilon_1\epsilon_2) - (\epsilon_1 k_2)(\epsilon_2 k_1)$ and $(\epsilon_1^\mu\epsilon_2^\nu T^{(2)}_{\mu\nu}) = 2s(\epsilon_1\Delta)(\epsilon_2\Delta) - (t-u)^2(\epsilon_1\epsilon_2) - 2(t-u)[(\epsilon_1\Delta)(\epsilon_2 k_1) - (\epsilon_1 k_2)(\epsilon_2\Delta)]$, with $\Delta^\mu \equiv p_1^\mu - p_2^\mu$ and ϵ_i the photon polarization vectors.

In χPT, the neutral $\pi\pi$ channel has no contribution at $\mathcal{O}(p^2)$, and at $\mathcal{O}(p^4)$ there is no tree-level, but only one-loop diagrams. Thus, at large-N_C the contributions to the $\gamma\gamma \to \pi^0\pi^0$ amplitude start at $\mathcal{O}(p^6)$ and read [21, 22]

$$\begin{aligned} A(s,t,u)^{\gamma\gamma\to\pi^0\pi^0} &= \frac{1}{(4\pi F)^4}\,(a_1 m_\pi^2 + a_2 s) \;+\; \mathcal{O}(E^4)\,, \\ B(s,t,u)^{\gamma\gamma\to\pi^0\pi^0} &= \frac{b}{(4\pi F)^4} \;+\; \mathcal{O}(E^2)\,, \end{aligned} \tag{3.15}$$

with $s,t,u,m_\pi^2 = \mathcal{O}(E^2)$. Since our holographic approach does not incorporate quark masses, the term with a_1 is out of the reach of the present work, and we focus on observables that do not contain it. In (3.15) the parameters a_2 and b are combinations

of LEC's. For three flavors and symmetry group $SU(3)$, the electric charge matrix is Q=diag$(2/3,-1/3,-1/3)$, and one finds the large–N_C low-energy parameters

$$a_2 = \frac{10}{9}\times 256\pi^4 F^2\Big(8C_{53}+8C_{55}+C_{56}+C_{57}+2C_{59}\Big)$$
$$b = -\frac{10}{9}\times 128\pi^4 F^2\Big(C_{56}+C_{57}+2C_{59}\Big)\,. \qquad (3.16)$$

In the holographic calculation [9] we obtained predictions for the $\mathcal{O}(p^6)$ LEC's, which yield particularly simple expressions,

$$a_2 = \frac{10}{9}\times 3N_C^2F^2\sum_n\frac{c_{v^n}^2}{m_{v^n}^2} \;=\; \frac{10}{9}\times N_C^2$$
$$b = \frac{10}{9}\times\frac{N_C^2F^2}{2}\sum_n\frac{c_{v^n}^2}{m_{v^n}^2} \;=\; \frac{10}{9}\times\frac{N_C^2}{6} \qquad (3.17)$$

using the sum-rule $\sum_n c_{v^n}^2/m_{v^n}^2=\sum_n g_{v^n\pi\pi}^2/m_{v^n}^2=1/(3F^2)$ derived in [9].

At higher energy it is possible to express our holographic result for the massless quark case in terms of the same function $h(Q^2)$:

$$A(s,t,u)^{\gamma\gamma\to\pi^0\pi^0} = \frac{a_2}{(4\pi F)^4}\left[\frac{(s-4t)}{2}\sum_n\frac{F^2c_{v^n}^2}{m_{v^n}^2-t} \;+\; (t\leftrightarrow u)\right]$$
$$= \frac{a_2}{(4\pi F)^4}\left[\frac{(s-4t)}{8}F^2h(-t) \;+\; (t\leftrightarrow u)\right]$$
$$= \frac{a_2}{(4\pi F)^4}\left[s \;+\; \frac{4L_1}{F^2}(8tu-5s^2) \;+\; \mathcal{O}(E^6)\right], \qquad (3.18)$$

$$B(s,t,u)^{\gamma\gamma\to\pi^0\pi^0} = \frac{b}{(4\pi F)^4}\left[\frac{3}{2}\sum_n\frac{F^2c_{v^n}^2}{m_{v^n}^2-t} \;+\; (t\leftrightarrow u)\right]$$
$$= \frac{b}{(4\pi F)^4}\left[\frac{3}{8}F^2h(-t) \;+\; (t\leftrightarrow u)\right]$$
$$= \frac{b}{(4\pi F)^4}\left[1 \;-\; \frac{12L_1s}{F^2} \;+\; \mathcal{O}(E^4)\right], \qquad (3.19)$$

with a_2 and b given in Eq. (3.17) and the low-energy expansion of $h(Q^2)$ in (3.8). We have kept the chiral expansion up to $\mathcal{O}(p^8)$, as later we will analyze the polarizability $(\alpha_2+\beta_2)$ which starts at that order at large–N_C.

For $N_C\to\infty$ the strange quark does not play a role in this amplitude and our holographic description yields the same prediction in $U(2)$ and $U(3)$. Moreover, since in the external legs we only have pions and non-singlet components in the electromagnetic gauge field ($J_\mu^{\rm em}=J_\mu^3+\frac{1}{\sqrt{3}}J_\mu^8$), the $U(3)$ result is identical to the $SU(3)$ one. It is clarifying to observe the $\gamma\to\pi V$ vertex obtained from the Lagrangian (2.12) in the $SU(3)$ case,

$$\mathcal{L} = \sum_n\frac{eN_Cc_{v^n}}{8\pi^2F}\,\epsilon^{\rho\sigma\mu\nu}\partial_\rho V_\sigma^{\rm em}\left[\frac{1}{3}\Big(\partial_\mu\pi^0\,\rho_\nu^{0,n}+\partial_\mu\pi^+\,\rho_\nu^{-,n}+\partial_\mu\pi^-\,\rho_\nu^{+,n}\Big)+\partial_\mu\pi^0\,\omega_\nu^n\right] \;+\; ... \qquad (3.20)$$

coincides with the one found in previous approaches based on resonance Lagrangians [33, 34].

If we restrict ourselves to $SU(2)$ with Q=diag$(1/2,-1/2)$ (but allowing the $SU(2)$ singlet resonance ω), all the $\rho^{\pm,0}$ terms vanish and only the ω resonance exchange survives. Thus, the $\mathcal{O}(p^6)$ χPT contribution at large N_C [22],

$$\begin{aligned} a_2 &= 256\pi^4 F^2 \Big(8C_{53} + 8C_{55} + C_{56} + C_{57} + 2C_{59} \Big) , \\ b &= -128\pi^4 F^2 \Big(C_{56} + C_{57} + 2C_{59} \Big) , \end{aligned} \tag{3.21}$$

becomes [9]

$$a_2 = N_C^2 \quad , \qquad\qquad b = \frac{N_C^2}{6} \quad . \tag{3.22}$$

Notice that we have used the $SU(3)$ notation for the corresponding $SU(2)$ couplings at large N_C. In $SU(2)$ notation one would have to make the replacement $C_{53} \to c_{29}$, $C_{55} \to c_{30}$, $C_{56} \to c_{31}$, $C_{57} \to c_{32}$ and $C_{59} \to c_{33}$ [19]. In the following phenomenological analysis we always consider the large–N_C estimates with the charge matrix Q=diag$(2/3,-1/3,-1/3)$.

3.2.2 $\gamma\gamma \to \pi^+\pi^-$

The charged pion mode contains the Born term at $\mathcal{O}(p^2)$ in the chiral expansion, given by the pion exchange diagram. At $\mathcal{O}(p^4)$ there is a tree-level contribution proportional to $(L_9 + L_{10})$ and one-loop diagrams. Hence, at large-N_C (where loop diagrams provide a subleading contribution) we have the chiral expansion [21–24]:

$$\begin{aligned} A(s,t,u)^{\gamma\gamma\to\pi^+\pi^-} &= \frac{1}{m_\pi^2 - t} + \frac{1}{m_\pi^2 - u} + \frac{8(L_9 + L_{10})}{F^2} + \frac{(a_1 m_\pi^2 + a_2 s)}{(4\pi F)^4} + \mathcal{O}(E^4) , \\ B(s,t,u)^{\gamma\gamma\to\pi^+\pi^-} &= \frac{1}{2s}\left[\frac{1}{m_\pi^2 - t} + \frac{1}{m_\pi^2 - u}\right] + \frac{b}{(4\pi F)^4} + \mathcal{O}(E^2) , \end{aligned} \tag{3.23}$$

with $s, t, u, m_\pi^2 = \mathcal{O}(E^2)$. In the three-flavor $SU(3)$ case, a_2 and b are given by the combinations of $\mathcal{O}(p^6)$ LEC's,

$$\begin{aligned} a_2 &= \frac{10}{9} \times 256\pi^4 F^2 \Big(8C_{53} - \frac{4}{5} \times 8C_{55} + C_{56} + C_{57} - \frac{4}{5} \times 2C_{59} \\ &\qquad + \frac{9}{10} \times 4C_{78} + \frac{9}{10} \times 8C_{87} - \frac{9}{10} \times 4C_{88} \Big) , \\ b &= -\frac{10}{9} \times 128\pi^4 F^2 \Big(C_{56} + C_{57} - \frac{4}{5} \times 2C_{59} - \frac{9}{10} \times 4C_{78} \Big) . \end{aligned} \tag{3.24}$$

Using the results for the $\mathcal{O}(p^6)$ LEC's in [9], we obtain the low-energy predictions

$$\begin{aligned} a_2 &= \frac{1}{9} \times 3N_C^2 F^2 \sum_n \frac{c_{v^n}^2}{m_{v^n}^2} = \frac{1}{9} \times N_C^2 , \\ b &= \frac{1}{9} \times \frac{N_C^2 F^2}{2} \sum_n \frac{c_{v^n}^2}{m_{v^n}^2} = \frac{1}{9} \times \frac{N_C^2}{6} . \end{aligned} \tag{3.25}$$

At higher energies it is possible to express the holographic result for massless quarks in terms of the function $h(Q^2)$:

$$\begin{aligned}
\bar{A}(s,t,u)^{\gamma\gamma\to\pi^+\pi^-} &= \frac{a_2}{(4\pi F)^4}\left[\frac{(s-4t)}{2}\sum_n \frac{F^2 c_{v^n}^2}{m_{v^n}^2 - t} \;+\; (t\leftrightarrow u)\right] \\
&= \frac{a_2}{(4\pi F)^4}\left[\frac{(s-4t)}{8} F^2 h(-t) \;+\; (t\leftrightarrow u)\right] \\
&= \frac{a_2}{(4\pi F)^4}\left[s \;+\; \frac{4L_1}{F^2}(8tu - 5s^2) \;+\; \mathcal{O}(E^6)\right], \\
\bar{B}(s,t,u)^{\gamma\gamma\to\pi^+\pi^-} &= \frac{b}{(4\pi F)^4}\left[\frac{3}{2}\sum_n \frac{F^2 c_{v^n}^2}{m_{v^n}^2 - t} \;+\; (t\leftrightarrow u)\right] \\
&= \frac{b}{(4\pi F)^4}\left[\frac{3}{8} F^2 h(-t) \;+\; (t\leftrightarrow u)\right] \\
&= \frac{b}{(4\pi F)^4}\left[1 \;-\; \frac{12L_1 s}{F^2} \;+\; \mathcal{O}(E^4)\right],
\end{aligned} \tag{3.26}$$

where the $\mathcal{O}(p^2)$ pion exchange term has been removed in $\bar{A}^{\gamma\gamma\to\pi^+\pi^-}$ and $\bar{B}^{\gamma\gamma\to\pi^+\pi^-}$, the $\mathcal{O}(p^4)$ result $L_9 + L_{10} = 0$ has been used, and a_2 and b are given in Eq. (3.25).

As in the neutral channel, the strange quark does not play a role in this amplitude at large-N_C, and the holographic description yields the same prediction in $U(2)$, $SU(3)$ and $U(3)$. However, if we restrict ourselves to $SU(2)$ sources and take just the tripet component of the electromagnetic charge matrix Q=diag$(1/2, -1/2)$ there is no vector exchange, and one finds [9, 23]

$$\begin{aligned}
a_2 &= 256\pi^4 F^2\Big(8C_{53} - 8C_{55} + C_{56} + C_{57} - 2C_{59} + 4C_{78} + 8C_{87} - 4C_{88}\Big) \;=\; 0\,, \\
b &= -128\pi^4 F^2\Big(C_{56} + C_{57} - 2C_{59} - 4C_{78}\Big) \;=\; 0\,.
\end{aligned} \tag{3.27}$$

In these two equations we have used the $SU(3)$ notation for the corresponding $SU(2)$ couplings; in $SU(2)$ notation one should replace $C_{53} \to c_{29}$, $C_{55} \to c_{30}$, $C_{56} \to c_{31}$, $C_{57} \to c_{32}$, $C_{59} \to c_{33}$, $C_{78} \to c_{44}$, $C_{87} \to c_{50}$ and $C_{88} \to c_{51}$ [19].

3.3 $\gamma \to \pi^+\pi^-\pi^0$ amplitude

The amplitude $\gamma^* \to \pi^+\pi^-\pi^0$ is described in the form [35, 36]

$$\langle\, 0|J_\mu^{EM}|\pi^+(p_1)\pi^-(p_2)\pi^0(p_3)\,\rangle \;=\; i\,\epsilon_{\mu\nu\alpha\beta} p_1^\nu p_2^\alpha p_3^\beta\, \mathcal{F}^{3\pi}(q^2,s,t)\,, \tag{3.28}$$

with $q = p_1 + p_2 + p_3$ and $s = (p_1+p_2)^2$, $t = (p_1+p_3)^2$, $u = (p_2+p_3)^2$ (with $s+t+u = q^2$ in the massless pion case). In the holographic models, the second term in Eq. (2.12) gives the direct coupling of the vector meson to three pions, which contributes to $\mathcal{F}^{3\pi}(q^2,s,t)$ for $q^2 \neq 0$. When the photon is on-shell ($q^2 = 0$) the amplitude has a simple structure in the chiral limit:

$$\mathcal{F}^{3\pi}(0,s,t) = \mathcal{F}_0^{3\pi} \times \frac{F^2}{4}\Big[h(-s) \;+\; h(-t) \;+\; h(-u)\Big] \tag{3.29}$$

with $\mathcal{F}_0^{3\pi} = \frac{eN_C}{12\pi^2 F^3}$ [35, 36]. At low energies we recover the ChPT expression

$$\mathcal{F}^{3\pi}(0,s,t) = \mathcal{F}_0^{3\pi} \times \left[1 \;+\; \mathcal{O}(E^4)\right], \tag{3.30}$$

since the $\mathcal{O}(E^2)$ term cancels due to the relation $s+t+u=0$ for massless pions.

In principle, further analyses could be considered for the decay $\eta \to \gamma\pi^+\pi^-$. The study of this flavor structure might allow the extraction of information about the $\mathcal{O}(p^6)$ couplings $C^W_{13,14,15}$, relevant for this kind of radiative processes [36].

3.4 Relations among the scattering amplitudes through holography

Before proceeding with the phenomenological analysis, it is interesting to summarize the holographic results for the massless quark limit, remarking how the various amplitudes are provided by the same Green's function integral $h(Q^2)$.

$\pi^+\pi^- \to \pi^0\pi^0$ scattering amplitude

$$A(s,t,u) = \frac{(t+2s)}{4}\, h(-t) \;+\; (t \leftrightarrow u)\,. \tag{3.31}$$

$\gamma\gamma \to \pi^0\pi^0$ amplitude

$$\begin{aligned} A(s,t,u)^{\gamma\gamma\to\pi^0\pi^0} &= \frac{a_2}{(4\pi F)^4}\left[\frac{(s-4t)}{8}\, F^2 h(-t) \;+\; (t \leftrightarrow u)\right], \\ B(s,t,u)^{\gamma\gamma\to\pi^0\pi^0} &= \frac{b}{(4\pi F)^4}\left[\frac{3}{8}\, F^2 h(-t) \;+\; (t \leftrightarrow u)\right]. \end{aligned} \tag{3.32}$$

The amplitude with charged pions has the same structure, up to a global factor, with the addition of the Born pion-exchange term.

$\gamma \to \pi^+\pi^-\pi^0$ radiative process

$$\mathcal{F}^{3\pi}(0,s,t) = \mathcal{F}_0^{3\pi} \times \frac{F^2}{4}\left[h(-s) \,+\, h(-t) \,+\, h(-u)\right]. \tag{3.33}$$

All the above scattering amplitudes are calculated in the 4D picture, i.e., using the resonances expansion. Since the results are all expressed in terms of the 5D Green's function, it would be interesting to see if they can be directly obtained from the five-dimensional action, a derivation still missing at present.

4 Polarizabilities and cross sections for $\gamma\gamma \to \pi\pi$ scattering

The polarizabilities can be defined following the notations provided by Refs. [22, 23]. The helicity amplitudes are written as

$$\begin{aligned} H_{++} &= A(s,t,u)^{\gamma\gamma\to\pi\pi} + 2(4m_\pi^2 - s)B(s,t,u)^{\gamma\gamma\to\pi\pi}\,, \\ H_{+-} &= \frac{8(m_\pi^4 - tu)}{s} B(s,t,u)^{\gamma\gamma\to\pi\pi}\,. \end{aligned} \tag{4.1}$$

which determine the $\gamma\gamma \to \pi\pi$ cross section

$$\sigma = \frac{\alpha^2\pi}{2s^2}\int_{t_-}^{t_+} dt\, H(s,t)\,, \tag{4.2}$$

with $H = |H_{++}|^2 + |H_{+-}|^2$, $t_\pm = m_\pi^2 - \frac{s}{2}(1 \mp \beta(s)Z)$, $\beta(s) = \sqrt{1-4m_\pi^2/s}$, for scattering angles in the range $|\cos\theta| < Z \leq 1$. The Mandelstam variables are $t = (p_1 - k_1)^2 = m_\pi^2 - \frac{s}{2}(1-\beta(s)\cos\theta)$ and $u = (p_2 - k_1)^2 = m_\pi^2 - \frac{s}{2}(1+\beta(s)\cos\theta)$, with $\vec{k}_1\cdot\vec{p}_1 = |\vec{k}_1|\,|\vec{p}_1|\,\cos\theta$. They obey the relation $s + t + u = 2m_\pi^2$.

At $\mathcal{O}(p^2)$ in χPT the neutral channel is zero and the charged one is provided by the Born term, $A^{\rm Born} = \frac{1}{m_\pi^2 - t} + \frac{1}{m_\pi^2 - u} = 2\,s\,B^{\rm Born}$ (Fig. 1a). This already provides a fairly good description of the experimental $\gamma\gamma \to \pi^+\pi^-$ data as one can see in Fig. 2. In our holographic approach one also has vector resonance exchanges in the crossed channel (Fig. 1c), although it is possible to observe in Fig. 2 that these corrections are tiny even at high energies. The neutral channel gets its first contribution at $\mathcal{O}(p^4)$ in the chiral expansion via one-loop diagrams (Fig. 1b). No tree-level diagram contributes at this order, and the loops are UV finite. Hence, we have a competition between the dominant chiral order in $\gamma\gamma \to \pi^0\pi^0$, $\mathcal{O}(p^4)$, which is subleading in $1/N_C$, and the dominant contribution at large–N_C, given by the vector exchanges and starting at $\mathcal{O}(p^6)$. As one can see in Fig. 3, near threshold the one-loop $\mathcal{O}(p^4)$ [24] contribution dominates, but as the energy increases the tree and loop diagrams interfere and the description improves at higher energies. We remark the importance of this interference, since just the resonance exchanges undervalue the cross section in the energy range below 800 MeV. Data from MARK-II [37], CELLO [38], Crystal Ball [39] and BELLE [40, 41] are compared to our theoretical estimates in Figs. 2 and 3. In particular, we provide the holographic results for the "Cosh" model; the results for the Hard-Wall model are practically identical and could not be distinguished in the plots.

The low-energy expansion of the helicity amplitudes for $t = m_\pi^2$ provides the polarizabilities [22, 23]:

$$\begin{aligned} \frac{\alpha}{m_\pi} H_{++}(s, t = m_\pi^2) &= \frac{\alpha}{m_\pi}\left[A^{\gamma\gamma\to\pi\pi} + 2(4m_\pi^2 - s)B^{\gamma\gamma\to\pi\pi}\right]_{t=m_\pi^2} \\ &\overset{s\to 0}{=} (\alpha_1 - \beta_1) + \frac{s}{12}(\alpha_2 - \beta_2) + \mathcal{O}(s^2)\,, \\ \frac{\alpha}{m_\pi} H_{+-}(s, t = m_\pi^2) &= \frac{\alpha}{m_\pi} 8m_\pi^2 B^{\gamma\gamma\to\pi\pi}\Big|_{t=m_\pi^2} \\ &\overset{s\to 0}{=} (\alpha_1 + \beta_1) + \frac{s}{12}(\alpha_2 + \beta_2) + \mathcal{O}(s^2)\,. \end{aligned} \tag{4.3}$$

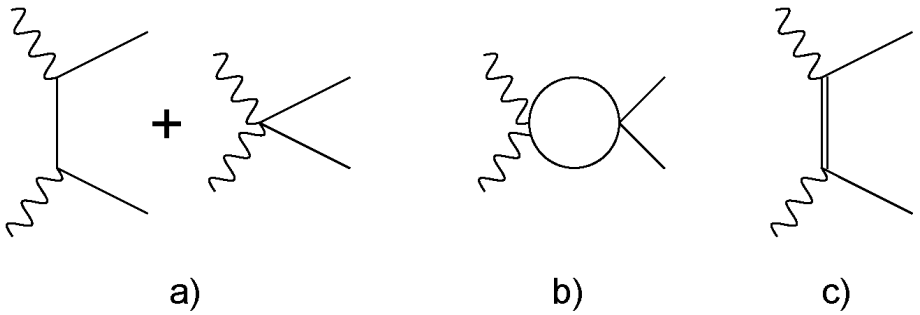

Figure 1. Feynman diagrams for $\gamma\gamma \to \pi\pi$: a) $\mathcal{O}(p^2)$ and $\mathcal{O}(p^4)$ tree-level (only in the charged channel), b) example of $\mathcal{O}(p^4)$ loops, c) vector resonance exchanges ($\mathcal{O}(p^6)$ and higher in our holographic approach). No other resonance diagram contributes in our analysis. The wavy, solid and double lines stand for photons, pions and vector resonances, respectively.

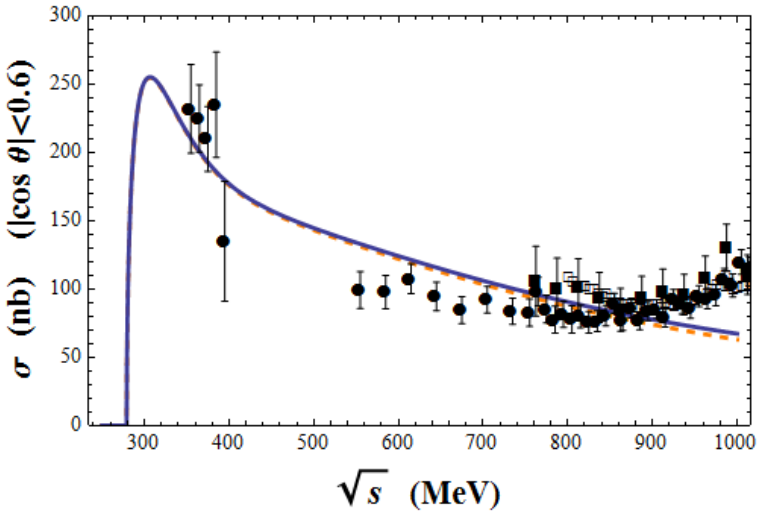

Figure 2. $\gamma\gamma \to \pi^+\pi^-$ cross section compared to our large-N_C expressions. The dashed green line is obtained from the Born term with one-pion exchange, which is $\mathcal{O}(p^2)$ in the χPT counting. In the holographic approach we have also vector exchanges, but their effect is essentially negligible even at high energies, as one can observe considering the full prediction in the "Cosh" model (solid blue curve). The data points are from MARK-II (circles) [37], CELLO (filled squares) [38], and BELLE experiment (empty squares) [40].

In the case of the charged pion amplitude, the Born term is subtracted when defining the polarizabilities.

The chiral expansion for the $\gamma\gamma \to \pi^0\pi^0$ polarizabilities are [22]:

$$
\begin{aligned}
(\alpha_1 - \beta_1)_{\pi^0} &= \frac{\alpha}{m_\pi}\frac{1}{(4\pi F)^2}\left\{ -\frac{1}{3} + \left(a_1^r + 8b^r + \mathcal{O}(p^6)\text{ loops}\right)\frac{m_\pi^2}{(4\pi F)^2} + \mathcal{O}(m_\pi^4)\right\},\\
(\alpha_1 + \beta_1)_{\pi^0} &= \frac{\alpha}{m_\pi}\frac{m_\pi^2}{(4\pi F)^4}\left\{ \left(8b^r + \mathcal{O}(p^6)\text{ loops}\right) + \mathcal{O}(m_\pi^2)\right\},\\
(\alpha_2 - \beta_2)_{\pi^0} &= \frac{\alpha}{m_\pi}\frac{1}{m_\pi^2(4\pi F)^2}\left\{\frac{156}{45} + \left(12a_2^r - 24b^r + \mathcal{O}(p^6)\text{ loops}\right)\frac{m_\pi^2}{(4\pi F)^2} + \mathcal{O}(m_\pi^4)\right\},\\
(\alpha_2 + \beta_2)_{\pi^0} &= \frac{\alpha}{m_\pi}\frac{1}{(4\pi F)^4}\left\{ \left(\mathcal{O}(p^6)\text{ loops}\right) + \mathcal{O}(m_\pi^2)\right\},
\end{aligned}
\tag{4.4}
$$

where the $\mathcal{O}(m_\pi^4)$ and $\mathcal{O}(m_\pi^2)$ terms at the end of each equation represent the contributions of $\mathcal{O}(p^8)$ and higher in χPT.

For the $\gamma\gamma \to \pi^+\pi^-$ polarizabilities one has the chiral expansion [21, 23]

$$
\begin{aligned}
(\alpha_1 - \beta_1)_{\pi^+} &= \frac{\alpha}{m_\pi}\frac{1}{(4\pi F)^2}\left\{ \frac{2\bar{\ell}_\Delta}{3} + \left(a_1^r + 8b^r + \mathcal{O}(p^6)\text{ loops}\right)\frac{m_\pi^2}{(4\pi F)^2} + \mathcal{O}(m_\pi^4)\right\},\\
(\alpha_1 + \beta_1)_{\pi^+} &= \frac{\alpha}{m_\pi}\frac{m_\pi^2}{(4\pi F)^4}\left\{ \left(8b^r + \mathcal{O}(p^6)\text{ loops}\right) + \mathcal{O}(m_\pi^2)\right\},\\
(\alpha_2 - \beta_2)_{\pi^+} &= \frac{\alpha}{m_\pi}\frac{1}{m_\pi^2(4\pi F)^2}\left\{ 2 + \left(12a_2^r - 24b^r + \mathcal{O}(p^6)\text{ loops}\right)\frac{m_\pi^2}{(4\pi F)^2} + \mathcal{O}(m_\pi^2)\right\},\\
(\alpha_2 + \beta_2)_{\pi^+} &= \frac{\alpha}{m_\pi}\frac{1}{(4\pi F)^4}\left\{ \left(\mathcal{O}(p^6)\text{ loops}\right) + \mathcal{O}(m_\pi^2)\right\},
\end{aligned}
\tag{4.5}
$$

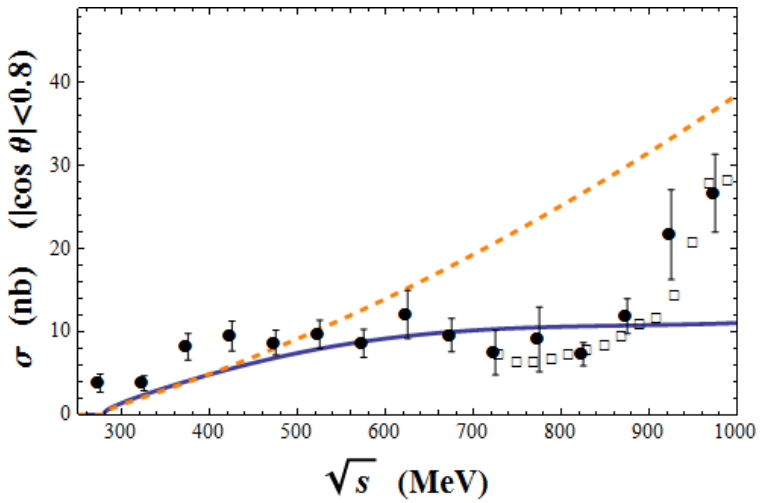

Figure 3. $\gamma\gamma \to \pi^0\pi^0$ cross section. Data from Crystal Ball [39] (circles) and BELLE [41] (empty squares) are compared to the $\mathcal{O}(p^4)$ χPT expression, which comes only from one-loop diagrams (dashed green). If we add the resonance contributions from the holographic "Cosh" model, we obtain the solid blue curve. One can appreciate the relevance of the pion loops at low energies, together with the importance of its interference with the vector meson exchanges at higher energy.

with $\bar{\ell}_\Delta = 192\,\pi^2(L_9(\mu)+L_{10}(\mu))$. Again, the $\mathcal{O}(m_\pi^4)$ and $\mathcal{O}(m_\pi^2)$ terms at the end of each equation represent the contributions of $\mathcal{O}(p^8)$ and higher in χPT. Since the a_1 parameter is out of the reach in our massless quark holographic approach, we focus on the combinations $(\alpha_1+\beta_1)$ and $(\alpha_2 \pm \beta_2)$.

At large N_C, in our holographic approach based on the $m_\pi \to 0$ limit, we have:

$$H_{++}(s,t=m_\pi^2) = \frac{a_2}{(4\pi F)^4}\left[\frac{2s}{3} + \mathcal{O}(s^2)\right],$$
$$H_{+-}(s,t=m_\pi^2) = \frac{b\,m_\pi^2}{(4\pi F)^4}\left[8 - \frac{96L_1 s}{F^2} + \mathcal{O}(s^2)\right]. \tag{4.6}$$

This leads to the large N_C determinations of the polarizabilities,

$$(\alpha_1+\beta_1) = \frac{\alpha}{m_\pi}\frac{8b\,m_\pi^2}{(4\pi F)^4} + \mathcal{O}(m_\pi^3),$$
$$(\alpha_2-\beta_2) = \frac{\alpha}{m_\pi}\frac{8a_2}{(4\pi F)^4} + \mathcal{O}(m_\pi),$$
$$(\alpha_2+\beta_2) = -\frac{\alpha}{m_\pi}\frac{1152L_1 b}{F^2}\frac{m_\pi^2}{(4\pi F)^4} + \mathcal{O}(m_\pi^3), \tag{4.7}$$

where we used the holographic prediction $a_2 = 6\,b$. Both the neutral and charged channels have the same structure and one must use the corresponding a_2 and b parameters. Notice that in the large N_C limit the polarizability $(\alpha_2+\beta_2)$ starts at $\mathcal{O}(p^8)$. In real world, the leading tree-level $\mathcal{O}(p^8)$ contribution obtained here competes with the $1/N_C$ suppressed $\mathcal{O}(p^6)$ loops.

It is convenient to keep track of the different contributions, and observe at which chiral order each of the polarizabilities begins. The first non-vanishing contribution appears at $\mathcal{O}(p^4)$ and comes from one-loop diagrams. Indeed, only $(\alpha_2-\beta_2)$ is different from zero at this order, and the other polarizabilities $(\alpha_1+\beta_1)$ and $\alpha_2+\beta_2)$ vanish [21–24]. The chiral expansion for $(\alpha_1+\beta_1)$ begins at $\mathcal{O}(p^6)$ (loop+tree-level) [21–23]. The polarizability $(\alpha_2+\beta_2)$ also starts at this order but only via loops, since the first tree-level contribution appears at $\mathcal{O}(p^8)$ [21–23].

At large N_C the first contribution to both $(\alpha_1+\beta_1)_{\pi^0}$ and $(\alpha_2-\beta_2)_{\pi^0}$ starts at $\mathcal{O}(p^6)$. The polarizability $(\alpha_2+\beta_2)_{\pi^0}$ is even more suppressed at large N_C, starting at $\mathcal{O}(p^8)$. In Table 2 we see how the values of the polarizabilities evolve as we include higher chiral orders. In the first column we provide the one-loop $\mathcal{O}(p^4)$ contributions [24] (the $\mathcal{O}(p^2)$ pion Born term is explicitly removed in the charged channel definitions and absent in the neutral one). Then we add the lowest order contribution from tree-level resonance exchanges from our holographic Lagrangian, $\mathcal{O}(p^6)$ for $(\alpha_1+\beta_1)$ and $(\alpha_2-\beta_2)$ and $\mathcal{O}(p^8)$ in the case of $(\alpha_2+\beta_2)$. Finally, in the last column we also sum up the $\mathcal{O}(p^6)$ loop contribution. We provide three numbers: the first one is given by $\bar{\ell}_3$ and $\bar{\ell}_4$ from [22, 23] and the values of $\bar{\ell}_{1,2,\Delta}$ extracted from $L_{1,2,3,9,10}(\mu)$ estimated from the "Cosh" model at $\mu = 770$ MeV; the second one is similar but with $\bar{\ell}_{1,2,\Delta}$ estimated from the Hard-Wall model; for the third number (in brackets) we have used the values of the $\mathcal{O}(p^4)$ LEC's from [22, 23] in the $\mathcal{O}(p^6)$ loop contribution. In the neutral channel one can see that the resonance contributions

seem to be slightly dominant with respect to the $\mathcal{O}(p^6)$ loops. However, vector resonance exchanges in the $\gamma\gamma \to \pi^+\pi^-$ amplitude carry a $\frac{1}{9}$ suppression factor and we found them of the same numerical size as the $\mathcal{O}(p^6)$ loops.

In Table 3 we compare the result in the last column of Table 2 to other determinations based on the Muskhelishvili-Omnès (MO) relation in terms of the $\pi\pi$–scattering phase-shifts [43] and to the χPT computation at $\mathcal{O}(p^6)$ [22, 23]. We obtain an overall agreement between the holographic determination and the MO and chiral computations. Further comparisons can be carried out with in previous experimental and theoretical results [42] collected in Table 4

We remark again that in our computation we have considered the charge matrix Q=diag($\frac{2}{3}, -\frac{1}{3}, -\frac{1}{3}$) in the calculation of our large–N_C estimates of the LEC's. Nonetheless, we have found a relatively good numerical agreement with the next-to-next-to-leading order (NNLO) χPT calculations from Refs. [22, 23], which rather considered the $SU(2)$ charge matrix Q=diag($\frac{1}{2}, -\frac{1}{2}$).

	$\mathcal{O}(p^4)$	$\mathcal{O}(p^4)$ + resonance (hologr.)	$\mathcal{O}(p^4)$ + reson. (hologr.) + $\mathcal{O}(p^6)$ loops
$(\alpha_1+\beta_1)_{\pi^0}$	0	0.58	0.75 ; 0.74 ; [0.69]
$(\alpha_2-\beta_2)_{\pi^0}$	20.73	27.67	30.18 ; 29.98 ; [34.65]
$(\alpha_2+\beta_2)_{\pi^0}$	0	-0.24	-0.16 ; -0.17 ; [-0.20]
$(\alpha_1+\beta_1)_{\pi^+}$	0	0.06	0.16 ; 0.16 ; [0.08]
$(\alpha_2-\beta_2)_{\pi^+}$	11.96	12.65	14.23 ; 14.12 ; [17.08]
$(\alpha_2+\beta_2)_{\pi^+}$	0	-0.02	0.03 ; 0.02 ; [-0.02]

Table 2. Polarizabilities in units of 10^{-4} fm^3 for α_1, β_1, and 10^{-4} fm^5 for α_2, β_2. They are provided at $\mathcal{O}(p^4)$ in the second column whereas in the third column we add the resonance contribution from the holographic models, which begins at $\mathcal{O}(p^6)$ for $(\alpha_1+\beta_1)$ and $(\alpha_2-\beta_2)$, and at $\mathcal{O}(p^8)$ in the χPT expansion for $(\alpha_2-\beta_2)$. The $\mathcal{O}(p^6)$ loop contributions are finally added in the last column.

5 Conclusions

Following previous analyses [1, 9], we have determined a novel set of relations between QCD matrix elements using holographic models where chiral symmetry is broken through IR b.c.'s. We have focused on the scattering amplitudes of pions and photons, finding that the three processes $\pi\pi \to \pi\pi$, $\gamma\gamma \to \pi\pi$ and $\gamma \to \pi\pi\pi$ involve a single scalar function $h(Q^2)$. This function is given by a suitable 5D integral of the EoM Green's function and accepts the usual decomposition in terms of resonance exchanges. Furthermore, in the considered processes only the vector mesons contribute (scalars and resonances of spin $S \geq 2$ are not included in the present approach).

In a detailed phenomenological analysis of $\gamma\gamma \to \pi\pi$ we have found an overall agreement with the experimental cross section for a broad range of energy. Likewise, the computed

	$\mathcal{O}(p^4)$ + reson. (hologr.) + $\mathcal{O}(p^6)$ loops	MO analysis [43]	NNLO χPT [22, 23]
$(\alpha_1+\beta_1)_{\pi^0}$	0.75 ; 0.74 ; [0.69]	$1.22 \pm 0.12 \pm 0.03$	1.1 ± 0.3
$(\alpha_2-\beta_2)_{\pi^0}$	30.18 ; 29.98 ; [34.65]	$32.1 \pm 0.9 \pm 1.9$	37.6 ± 3.3
$(\alpha_2+\beta_2)_{\pi^0}$	-0.16 ; -0.17 ; [-0.20]	$-0.19 \pm 0.02 \pm 0.01$	0.04
$(\alpha_1+\beta_1)_{\pi^+}$	0.16 ; 0.16 ; [0.08]	$0.19 \pm 0.09 \pm 0.03$	0.16 [0.16]
$(\alpha_2-\beta_2)_{\pi^+}$	14.23 ; 14.12 ; [17.08]	$14.7 \pm 1.5 \pm 1.4$	16.2 [21.6]
$(\alpha_2+\beta_2)_{\pi^+}$	0.03 ; 0.02 ; [-0.02]	$0.11 \pm 0.03 \pm 0.01$	-0.001

Table 3. Our holographic predictions for the polarizabilities provided in the second column (same outcomes as in the last column in Table 2) compared to results from the MO representation [43] and to the NNLO χPT analyses [22, 23]. Units are the same as in Table 2.

	CELLO [38, 45]	MARK-II [37, 45]	Crystal Ball [39, 45]	Vector exchanges [33, 34]	Sum rules [44]
$(\alpha_1+\beta_1)_{\pi^0}$			1.00 ± 0.05	0.83	0.802 ± 0.035
$(\alpha_2-\beta_2)_{\pi^0}$					39.72 ± 8.01
$(\alpha_2+\beta_2)_{\pi^0}$					-0.171 ± 0.067
$(\alpha_1+\beta_1)_{\pi^+}$	0.30 ± 0.04	0.22 ± 0.06		0.07	0.166 ± 0.024
$(\alpha_2-\beta_2)_{\pi^+}$					25.75 ± 7.03
$(\alpha_2+\beta_2)_{\pi^+}$					0.121 ± 0.064

Table 4. Pion polarizabilities from experimental measurements [37–39, 45] and theoretical analyses [33, 34, 44]. Units are the same as in Table 2.

polarizabilities at low energies show a fair agreement between the holographic approach, previous computations and experiment.

Acknowledgments

We thank Fulvia De Fazio, Juerg Gasser, Floriana Giannuzzi, Mihail Ivanov and Stefano Nicotri for useful discussions. This work is partially supported by the Italian Miur PRIN 2009, the Universidad CEU Cardenal Herrera grant PRCEUUCH35/11, the MICINN-INFN fund AIC-D-2011-0818, and by the National Natural Science Foundation of China under Grant No. 11135011.

A Constraints on the background functions

Here we provide constraints on the background functions $f^2(z)$ and $g^2(z)$. As proposed in ref. [10], these functions must be invariant under the reflection of z in order to properly

define the parity. More constraints come from the results for the low-energy constants.

With the resonance decomposition of the gauge potential (2.6), up to $\mathcal{O}(p^4)$ the 5D Yang-Mills action reduces to the χPT Lagrangian [9, 11, 12]:

$$\begin{aligned} S_2[\pi]+S_4[\pi] = \int d^4x \Bigg[& \frac{F^2}{4} < u_\mu u^\mu > \\ & + L_1 < u_\mu u^\mu >^2 + L_2 < u_\mu u_\nu >< u^\mu u^\nu > + L_3 < u_\mu u^\mu u_\nu u_\nu > \\ & - i L_9 < f_{+\mu\nu} u^\mu u^\nu > + \frac{L_{10}}{4} < f_{+\mu\nu} f_+^{\mu\nu} - f_{-\mu\nu} f_-^{\mu\nu} > \\ & + \frac{H_1}{2} < f_{+\mu\nu} f_+^{\mu\nu} + f_{-\mu\nu} f_-^{\mu\nu} > \Bigg] . \end{aligned} \tag{A.1}$$

The low-energy constants in (A.1) are given by the 5D integrals

$$\begin{aligned} F^2 &= 4 \left(\int_{-z_0}^{z_0} \frac{\mathrm{d}z}{f^2(z)} \right)^{-1} , \\ L_1 &= \frac{1}{2} L_2 = -\frac{1}{6} L_3 = \frac{1}{32} \int_{-z_0}^{z_0} \frac{(1-\psi_0^2)^2}{g^2(z)} \, \mathrm{d}z \, , \\ L_9 &= -L_{10} = \frac{1}{4} \int_{-z_0}^{z_0} \frac{1-\psi_0^2}{g^2(z)} \, \mathrm{d}z \, , \\ H_1 &= -\frac{1}{8} \int_{-z_0}^{z_0} \frac{1+\psi_0^2}{g^2(z)} \, \mathrm{d}z \, . \end{aligned} \tag{A.2}$$

We demand that all these integrals except H_1 are finite. For H_1, which is the coefficient of the kinetic term of the external sources, we require it to be divergent. From the finiteness of the pion decay constant F we find the solution

$$\psi_0(z) = \frac{F^2}{2} \int_0^z \frac{1}{f^2(z)} \mathrm{d}z \ , \tag{A.3}$$

which satisfies the equation of motion with boundary conditions $\psi_0(\pm z_0) = \pm\, 1$. Since $\psi_0(z)$ is a monotonic function of z, we can choose it as the coordinate parameter through a coordinate transformation in z. Defining $y = \psi_0(z)$, it is not difficult to find the new background functions

$$\tilde{f}^2(y) = \frac{F^2}{2}, \quad \tilde{g}^2(y) = \frac{F^2}{2} \frac{g^2(z(y))}{f^2(z(y))}, \tag{A.4}$$

together with the boundaries $y = \pm 1$. It turns out that this coordinate system is convenient in many respects, both for theoretical derivations and numerical calculations. In this coordinate system the integral for F becomes trivial, and the other integrals can be expressed as

$$\begin{aligned} L_1 &= \frac{1}{32} \int_{-1}^{1} \frac{(1-y^2)^2}{\tilde{g}^2(y)} \, \mathrm{d}y \ , \\ L_9 &= \frac{1}{4} \int_{-1}^{1} \frac{1-y^2}{\tilde{g}^2(y)} \, \mathrm{d}y \ , \\ H_1 &= -\frac{1}{8} \int_{-1}^{1} \frac{1+y^2}{\tilde{g}^2(y)} \, \mathrm{d}y \ . \end{aligned} \tag{A.5}$$

Requiring that L_1 and L_9 are finite and H_1 divergent, we get the constraint near the boundaries

$$(1-y^2)^2 < \tilde{g}^2(y) \leq C(1-y^2) \tag{A.6}$$

with C a constant. Actually, the explicit boundary behavior of the function, $\tilde{g}^2(y)$, can be used to clarify the ultraviolet property of different models. Among the models shown in the next appendix, this function behaves as $(1-y^2)^0$ in the flat model, related to a convergent value of H_1, while in the Sakai-Sugimoto model, it goes as $(1-y^2)^{4/3}$. As for all the asymptotic anti-de Sitter backgrounds, the equality in the above relation is exactly satisfied, e.g., in the "cosh" and Hard-Wall models.

In the new coordinate system, the quantity $\mathcal{H}$ defined in Eq. (3.12) simplifies as

$$\mathcal{H} = \frac{1}{4}\int_{-1}^{1} \tilde{g}^2(y)\,\mathrm{d}y \ , \tag{A.7}$$

and, with the constraint (A.6), it is finite.

B Holographic models

We have used four different holographic models, defined by the functions $f^2(z)$ and $g^2(z)$ and by the value of z_0. Here we list their details in each model. The expressions of the wave functions solutions of the equation of motion, and of other quantities like F, the couplings and the mass spectrum, can be found in the appendix of ref. [9].

"Flat" background [10]:

$$f^2(z) = \frac{\Lambda^2}{g_5^2} \ , \quad g^2(z) = g_5^2 \quad , \quad z_0 = 1. \tag{B.1}$$

"Cosh" model [10]:

$$f^2(z) = \frac{\Lambda^2 \cosh^2(z)}{g_5^2} \ , \quad g^2(z) = g_5^2 \ , \quad z_0 = \infty. \tag{B.2}$$

"Hard-wall" model [12]:

$$f^2(z) = \frac{1}{g_5^2(z_0 - |z|)} \ , \quad g^2(z) = g_5^2(z_0 - |z|) \ , \quad z_0 < \infty. \tag{B.3}$$

"Sakai-Sugimoto" model [11, 13]:

$$f^2(z) = \frac{\Lambda^2(1+z^2)}{g_5^2} \ , \quad g^2(z) = g_5^2(1+z^2)^{1/3} \ , \quad z_0 = \infty. \tag{B.4}$$

C Isospin and partial-wave projection in $\pi\pi$–scattering

The amplitude $A(s,t,u)$ provides the scattering amplitudes T^I of modes with definite isospin $I = 0, 1, 2$ [16, 30]:

$$
\begin{aligned}
T^0(s,t,u) &= 3A(s,t,u) + A(t,s,u) + A(u,s,t)\,, \\
T^1(s,t,u) &= A(t,s,u) - A(u,s,t)\,, \\
T^2(s,t,u) &= A(t,s,u) + A(u,s,t)\,.
\end{aligned} \tag{C.1}
$$

In the isospin $I = 2$ amplitude, there are no resonances in the s–channel, only exchanges in the crossed channels. This simplifications makes the amplitude particularly interesting for the study of its partial waves, which in the massless quark limit have the form [16, 30]

$$
\begin{aligned}
T^I_J(s) &= \frac{1}{32\pi s}\int_{-s}^{0} \mathrm{dt}\; P_J\left(1+\frac{2t}{s}\right) T^I(s,t,u) \\
&= \frac{1}{64\pi}\int_{-1}^{1} \mathrm{dx}\; P_J(x)\, T^I(s,-s(1-x)/2,-s(1+x)/2) \\
&= \frac{1}{32\pi}\int_{0}^{1} \mathrm{dy}\; P_J(1-2y)\, T^I(s,-sy,-s(1-y))\,,
\end{aligned} \tag{C.2}
$$

with $u = -s-t$ (in the chiral limit), $y = (1-x)/2 = -t/s$ and P_J the Legendre polynomials.

References

[1] D. T. Son and N. Yamamoto, [arXiv:1010.0718].

[2] P. Colangelo, F. De Fazio, J.J. Sanz-Cillero, F. Giannuzzi, and S. Nicotri, Phys. Rev. **D85** (2012) 035013 [arXiv:1108.5945].

[3] L. Cappiello, O. Catá, and G. D'Ambrosio, Phys. Rev. **D82** (2010) 095008 [arXiv:1004.2497].

[4] M. Knecht, S. Peris, and E. de Rafael, JHEP **1110** (2011) 048 [arXiv:1101.0706].

[5] S.K. Domokos, J.A. Harvey, and A.B. Royston, JHEP **1105** (2011) 107 [arXiv:1101.3315].

[6] R. Alvares, C. Hoyos, and A. Karch, Phys. Rev. **D84** (2011) 095020 [arXiv:1108.1191].

[7] A. Gorsky, P.N. Kopnin, A. Krikun, and A. Vainshtein, Phys. Rev. **D85** (2012) 086006 [arXiv:1201.2039].

[8] I. Iatrakis and E. Kiritsis, JHEP **1202** (2012) 064 [arXiv:1109.1282].

[9] P. Colangelo, J.J. Sanz-Cillero, and F. Zuo, JHEP **1211** (2012) 012 [arXiv:1207.5744].

[10] D. T. Son and M. A. Stephanov, Phys. Rev. **D69** (2004) 065020 [arXiv:hep-ph/0304182].

[11] T. Sakai and S. Sugimoto, Prog. Theor. Phys. **113** (2005) 843 [arXiv:hep-th/0412141].

[12] J. Hirn and V. Sanz, JHEP **12** (2005) 030 [arXiv:hep-ph/0507049].

[13] T. Sakai and S. Sugimoto, Prog. Theor. Phys. **114** (2005) 1083 [arXiv:hep-th/0507073].

[14] G. 't Hooft, Nucl. Phys. **B72** (1974) 461; **75** (1974) 461. E. Witten, Nucl. Phys.**B160** (1979) 57.

[15] S. Weinberg, Physica A **96** (1979) 327.

[16] J. Gasser and H. Leutwyler, Annals Phys. **158** (1984) 142; Nucl. Phys. B **250** (1985) 465, 517.

[17] J. Bijnens, G. Colangelo, and G. Ecker, JHEP **02** (1999) 020 [arXiv:hep-ph/9902437].

[18] J. Bijnens, G. Colangelo, and G. Ecker, Annals Phys. **280** (2000) 100 [arXiv:hep-ph/9907333].

[19] J. Bijnens, L. Girlanda, and P. Talavera, Eur. Phys. J. **C23** (2002) 539-544, [arXiv:hep-ph/0110400].

[20] T. Ebertshauser, H.W. Fearing, and S. Scherer, Phys. Rev. **D65** (2002) 054033, [arXiv:hep-ph/0110261].

[21] U. Burgi, Nucl.Phys. B **479** (1996) 392 [arXiv:hep-ph/9602429]; Phys.Lett. B **377** (1996) 147 [arXiv:hep-ph/9602421].

[22] J. Gasser, M. A. Ivanov, and M. E. Sainio, Nucl. Phys. **B728** (2005) 31 [arXiv:hep-ph/0506265].

[23] J. Gasser, M. A. Ivanov, and M. E. Sainio, Nucl. Phys. **B745** (2006) 84 [arXiv:hep-ph/0602234].

[24] J. Bijnens and F. Cornet, Nucl. Phys. **B296** (1988) 557.

[25] J. Wess and B. Zumino, Phys. Lett. **B37** (1971) 95.

[26] E. Witten, Nucl. Phys. **B223** (1983) 422, 433.

[27] G. Ecker, J. Gasser, A. Pich and E. de Rafael, Nucl. Phys. **B321** (1989) 311. G. Ecker, J. Gasser, H. Leutwyler, A. Pich and E. de Rafael, Phys. Lett. **B223** (1989) 425.

[28] V. Cirigliano, G. Ecker, M. Eidemüller, R. Kaiser, A. Pich and J. Portolés, Nucl. Phys. **B753** (2006) 139 [arXiv:hep-ph/0603205].

[29] J. Beringer *et al.* [Particle Data Group Collaboration], Phys. Rev. **D86** (2012) 010001.

[30] J. Bijnens, P. Dhonte and P. Talavera, JHEP **0401** (2004) 050. [arXiv:hep-ph/0401039].

[31] Z.H. Guo, J.J. Sanz-Cillero and H.Q. Zheng, Phys. Lett. **B661** (2008) 342 [arXiv:0710.2163 [hep-ph]].

[32] J. Nieves, A. Pich and E. Ruiz Arriola, Phys. Rev **D84** (2011) 096001 [arXiv:1107.3247 [hep-ph]].

[33] P. Ko, Phys. Rev. **D41** (1990) 1531.

[34] D. Babusci, S. Bellucci, G. Giordano, G. Matone, Phys. Lett. **B314** (1993) 112.

[35] J. Bijnens, A. Bramon and F. Cornet, Phys. Lett. B **237** (1990) 488

[36] T. Hannah, Nucl. Phys. B **593** (2001) 577 [arXiv:hep-ph/0102213]; O. Strandberg, [arXiv:hep-ph/0302064].

[37] J. Boyer *et al.* (MARK-II Coll.), Phys. Rev. **D 42** (1990) 1350.

[38] H.J. Behrend *et al.* (CELLO Coll.), Z. Phys. **C 56** (1992) 381.

[39] H. Marsiske et al. (Crystal Ball Collaboration), Phys. Rev. **D41** (1990) 3324.

[40] T. Mori et al. (Belle Collaboration), J. Phys. Soc. Jpn. **76** (2007) 074102 [arXiv:0704.3538]; T. Mori et al. (Belle Collaboration), Phys. Rev. **D 75** (2007) 051101 [arXiv:hep-ex/0610038].

[41] S. Uehara et al. (Belle Collaboration), Phys. Rev. **D 78** (2008) 052004 [arXiv:0805.3387]; S. Uehara et al. (Belle Collaboration), Phys. Rev. **D 79** (2009) 052009 [arXiv:0903.3697].

[42] For a review see: J. Portoles and M. R. Pennington, in *Maiani, L. (ed.) et al.: The second DAPHNE physics handbook, vol. 2* 579-596 [arXiv:hep-ph/9407295].

[43] R. Garcia-Martin and B. Moussallam, Eur. Phys. J. **C70** (2010) 155 [arXiv:1006.5373].

[44] L. V. Filikov, V. L. Kashevarov, Phys. Rev. **C72** (2005) 035211 [arXiv:nucl-th/0505058]; Phys. Rev. **C73** (2006) 035210 [arXiv:nucl-th/0512047].

[45] A.E. Kaloshin, V.M. Persikov and V.V. Serebryakov, Phys. Atom. Nucl. **57** (1994) 2207; Yad. Fiz. 57 N **12** (1994) 2298 [arXiv:hep-ph/9402220]. A.E. Kaloshin and V.V. Serebryakov, Z. Phys. **C 64** (1994) 689 [arXiv:hep-ph/9306224].